Temperature Calibration of the MINOS Calibration Detector

1st Year Report submitted to the
High Energy Physics Department of
University College london
by

David Jason Koskinen

[June 2005]

1 Introduction

John Bahcall and Ray Davis Jr. started the neutrino oscillation game with a 1963 experiment using dry cleaning fluid. They used a 100,000 gallon tank of the fluid to look at the rate of solar neutrino interactions in Homestake Mine, South Dakota. In 1968[1] the results were published that there existed a deficit in the expected number of solar neutrinos. Near the turn of the millenium experiments such as Super-Kamiokande[2] and the Sudbury Neutrino Observatory (SNO)[3] published very strong results that established a deficit of atmospheric neutrinos. With a deficit in both Solar and Atmospheric neutrinos the next step was to create a reliable and tunable source of neutrinos for examination of the neutrino disappearance phenomenon. The crown jewel of this new crop of beam neutrino experiments is the Main Injection Neutrino Oscillation Search (MINOS).

The quick and dirty explanation of the neutrino disappearance is that neutrinos oscillate to flavors that past experiments cannot/did not detect. Both SNO and Super-K have seen a depletion in charged current (CC) interactions, but there has been no deficiency in expected Neutral Current (NC) interactions in either solar or atmospheric neutrino studies. This result suggests oscillation over more exotic ideas such as neutrino decay, because NC events are flavor independent and the expected numbers of NC events are detected. CC events are flavor dependent and a depletion is detected. This rules out Neutrino decay because a $\frac{1}{3}$ depletion in just CC muon neutrino events should be accompanied by a $\frac{1}{6}$ depletion in NC events.

2 Oscillation Theory

Neutrinos are detected as flavor or weak eigenstates (ν_e, ν_μ, ν_τ), but composed and propagate as a superposition of the Neutrino mass eigenstates (ν_1, ν_2, ν_3); Electron neutrinos are predominantly ν_1, Muon Neutrinos are predominantly ν_2 and Tau Neutrinos are predominantly ν_3. While there is some mixing between all three flavor and mass eigenstates in the neutrino sector MINOS is probing a mixing mode between ν_μ and ν_τ and the mass eigenstates ν_2 and ν_3 with masses m_2 and m_3. The

relationship between weak and mass eigenstates is given as

$$\begin{pmatrix} |\nu_\tau\rangle \\ |\nu_\mu\rangle \end{pmatrix} = \mathcal{M} \begin{pmatrix} |\nu_3\rangle \\ |\nu_2\rangle \end{pmatrix} \tag{1}$$

or more precisely:

$$\begin{pmatrix} |\nu_\tau\rangle \\ |\nu_\mu\rangle \end{pmatrix} = \begin{pmatrix} cos\ \theta & sin\ \theta \\ -sin\ \theta & cos\ \theta \end{pmatrix} \begin{pmatrix} |\nu_3\rangle \\ |\nu_2\rangle \end{pmatrix} \tag{2}$$

where the mixing matrix $\mathcal{M}$ is unitary, and θ is the mixing angle between the mass and flavor eigenstates.

The NuMI beam will be producing Neutrinos that are mainly ν_μ with some cheeky ν_e slipping in through unwanted decays. This means that at the source, excluding the small amount of ν_e Neutrinos,

$$|\nu_{x=0}\rangle = |\nu_\mu\rangle = -sin\ \theta|\nu_3\rangle + cos\ \theta|\nu_2\rangle \tag{3}$$

This will describe the beam composition at its initial creation. After some time the probability of the evolving state $\nu_\mu(t)$ must also incorporate the time-evolution operator which gives the eigenvalue e^{-iEt}. With this new addition

$$|\nu_\mu(t)\rangle = -sin\theta e^{-iE_3t}|\nu_3\rangle + cos\theta e^{-iE_2t}|\nu_2\rangle \tag{4}$$

and the oscillation probability for $\nu_\mu \to \nu_\tau$ is:

$$\begin{aligned} P_{\nu_\mu\to\nu_\tau} &= |\langle\nu_\tau|\nu_\mu(t)\rangle|^2 \\ &= sin^2\theta cos^2\theta(2 - e^{-i(E_3-E_2)t} - e^{i(E_3-E_2)t} \\ &= 2sin^2\theta cos^2\theta(1 - cos(E_3 - E_2)t) \\ &= sin^2(2\theta)sin^2\tfrac{(E_3-E_2)t}{2} \end{aligned} \tag{5}$$

Knowing that E_1,$E_2 \gg m_1, m_2$, then:

$$E_2 - E_1 = \sqrt{{m_2}^2 + p^2} - \sqrt{{m_1}^2 + p^2} \approx \frac{{m_2}^2 - {m_1}^2}{2p}$$
$$p \approx E \tag{6}$$

and since Neutrinos are relativistic the approximation that $t \approx L$, where L is the length traveled, can also be used to succinctly bring together

$$P_{\nu_\mu \to \nu_\tau} \approx sin^2(2\theta) sin^2\left(\frac{\Delta {m_{32}}^2 L}{4E}\right) \tag{7}$$

When this equation is converted from natural units to expressing energy in GeV, Distance in km and mass in eV the probability reduces down to its final form:

$$P_{\nu_\mu \to \nu_\tau} = sin^2(2\theta) sin^2\left(\frac{1.27 \Delta {m_{32}}^2 L}{4E}\right) \tag{8}$$

This is the equation the elucidates the behavior of Neutrino oscillation and is the starting point for any Long-Baseline experiment such as MINOS. By setting or changing either the Length or Energy of a Neutrino beam, it is possible to examine the unknown values of the mixing angle θ and mass difference Δm^2.

3 Beam and Detectors

The MINOS experiment consists of a neutrino beam and three steel calorimeter detectors, the Far Detector, Near Detector and Calibration Detector. The Near Detector is located at Fermilab in Batavia, Illinois and is situated a couple hundred meters downstream of beam target and decay pipe. The Far Detector is situated 732 km from Fermilab in the Soudan Underground mine in Tower, Minnesota. The Calibration Detector resided at CERN in Geneva, Switzerland, until its dismantling in January 2004.

The beam is created when a spill of 120 GeV protons are diverted from the Main Injector and directed onto the MINOS target, 47 carbon fins ensconced in a water cooled target chamber. Pion's

and Kaons from the ensuing hadronic debris are focused via two parabolic magnetic horns down a decay tunnel where their decay chain finally ends in muon's and muon neutrinos.

The three MINOS detectors are similar in their detection of neutrino events to minimize potential systematic differences. All were assembled of modules of scintillator sandwiched between 1 inch thick steel planes. The Far Detector is as large as possible to be able to examine events from a neutrino beam that widens from tens of centimeters at the beam source, right before the Near Detector, to a diameter of a few kilometers on arrival at the Soudan mine. The Near Detector is smaller than the Far and adjusted to compensate for a significantly higher flux of events. The Calibration Detector used components from both the Near and Far Detectors to evaluate the different responsiveness of the Far and Near Detector electronics and setup under the same conditions.

3.1 Steel

The steel serves an array of needs for this experiment. First, it is necessitated as an absorbing layer for unwanted particles. Second, it provides the mass for a high energy neutrino to turn into an electron, tau or muon. Third, it is a ferromagnetic material and allows the Detectors to be magnetized. Lastly, it provides the anchoring structure for the scintillator modules to be attached. Without these benefits an experiment of this nature would be impossible.

3.2 Scintillator and Fibers

The scintillator modules are made of scintillator strips that measure 1 cm thick and 4.1 cm wide. The strips are placed side by side to construct Scintillator Modules. The whole module is encased in an Aluminum skin to prevent ambient light from entering the module and the modules are rotated 90° to the preceding module along the beam path to provide three dimensional tracking capabilities.

Photons created by the charged particle interaction with the scintillant are absorbed by a Wave-Length Shifting (WLS) fiber and transported down the length of a scintillator module. At the edge of the module there is clear optic cable that is attached to the outputs of the scintillator plane/WLS fiber and whose corresponding ends are bundled to shine out onto a photomultiplier Tube(PMT). The incoming light is separated to shine on specific sections of a PMT and thus the PMT has multiple

outputs corresponding to the individual location or 'pixel' upon which the light hit the PMT. The outputs of the PMT are run to a bevy of electronic equipment which record and manage the timing and energy deposition from an event.

4 CalDet Temperature Calibration

To make a significant measurement of Δm^2 and $sin^2 2\theta$, MINOS is targeting a 5% absolute calibration and a 2% relative calibration between the Near and Far Detector. The **Cal**ibration **Det**ector (CalDet) was a major project addressing this goal. Built in the Positron Synchrotron hall at CERN it was unmagnetized 1m x 1m x 3.6m version of the Near or Far Detector, that was utilized to test the responsiveness of the respective Near/Far detector electronics within a controlled environment. While both the Near and Far detector have a controlled environments the CalDet does not, and all measurements were subject to temperature fluctuations on the order. This is significant because the scintillator has a .3%/^{o}C light output shift that accompanied with a $\sim 10^oC$ daily change in temperature singly swallows the %2 relative calibration. To combat this anticipated issue a Radio Shack (RS) temperature probe was installed directly beneath the CalDet for the initial data taking runs, and in 2003 thermocouple (Data Control Systems - DCS) probes were attached to various parts of the detector to provide finer temperature resolution and a better picture of local fluctuations.

The goal was twofold in attaching the thermocouple probes to the CalDet. The RS probe laid on a bed of steel directly underneath the middle of the detector and was therefore susceptible to drafts entering the T7 or T11 beam area where the CalDet was situated. Thermocouples directly attached to the face of the steel plates would more accurately record the temperature of the detector instead of the surrounding air temperature. The second was that 60 planes of steel and scintillator have a heat capacity that will cause the responsiveness of the detector to lag behind the ambient temperature. Thermocouples when attached to the detector can be compared to thermocouples and the RS probe recording the ambient temperature to establish an offset.

4.1 Temp Work

A relative conversion between the RS and DCS probes was essential in order to use results from the thermocouple analysis to understand data taken exclusively with the RS probe. The first examination of DCS and RS versus time established a discrepancy between the absolute temperature scale registered by the RS probe and the DCS probe (fig 1). This can be corrected by finding the slope of the DCS vs RS slope and using that as a constant to convert RS temperatures to DCS temperatures. The DCS vs RS temperature plot (fig 2) was not a straight line and exhibited a structure that suggested two things:

- The DCS probes are heavily influenced by the CalDet temperature and the RS probe was more heavily influenced by the ambient temperature. This is established by a lack of a straight line.
- There is a hysteresis in the plot that shows an offset in temperature response. i.e. if DCS temp can be experimentally modeled as $t_1 = A_1 * sin(x + \phi_1)$ and DCS temp as $t_2 = A_2 * sin(x + \phi_2)$ then $|\phi_2 - \phi_1| > 0$. The RS probe was not measuring the temperature of the detector, but the ambient temperature of the detector hall.

The hysteresis in the plot shows that not only is the absolute calibration off, but the relative calibration is also off. The initial attempt to solve this problem revolved around plotting $sin^{-1}(t_1)$ vs. $sin^{-1}(t_2)$ to get rid of the x term and have just the phase(offsets) plotted against each other. For this to work A_1 and A_2 must be calculated so that the $\frac{sin^{-1}(A_1)}{sin^{-1}(A_2)}$ term is a known constant. Plots using all 24 thermocouples, during 10 days of the Near/Far run, over only a 'linear' region of DCS vs RS temp were used to find heating and cooling slopes (fig 3. In these regions the respective sin() terms should be approximately equal and the slope will establish the $\frac{A_1}{A_2}$ constant which can be used to calculate the $\frac{sin^{-1}(A_1)}{sin^{-1}(A_2)}$ term, which is needed to find the offset. This work came to a grinding halt when it encountered two issues:

- The cooling/heating analysis showed a heating value ($\sim \frac{A_1}{A_2}$) of $1.956 \pm .307$ while the cooling value was $1.716 \pm .385$. This shows that the amplitudes of A1 and A2 change and do not consistently scale i.e. A1 = 1.7*A2 is not always true throughout a 24 period.

- DCS and RS temperature are not perfectly sinusoidal or even smooth over a 24 hour period. In a completely enclosed space devoid of random temperature changes from doors opening/closing or drafts, modeling becomes possible. In the meantime the data is routinely jumpy and this makes any mathematical approximation approach to this problem subject to extreme error.

A more robust analysis that avoids the above mentioned pitfalls is that of utilizing a running average to establish the offset. The method uses X DCS vs RS temperature points whose slope is averaged to see at what time of day the running average differs more than .2 from the previously calculated heating slope average using all the thermocouples (fig 4). The time is noted and the running average slope is calculated until it agrees with the cooling slope to within .2, thereby giving the offset as $\frac{B-A}{2}$. In theory this is a strong analysis, but the data is too jumpy for consistently reliable results. Fig 5 shows an instance where the method works, while fig 6 exhibits when the method does not work.

Unfortunately a show-stopper was encountered that would have ruined any successful results from any analysis to get a DCS to RS conversion. The problem stemmed from thermocouples having two leads (brown, tan) that were entered into a National Instruments Field Point Unit to record the voltage. Reversing the brown or tan lead in a thermocouple created non-linearity when examined versus a thermocouple of opposite orientation (fig 7). This meant that if the leads of thermocouple 2 were reversed from that of thermocouple 3, a plot of DCS 2 vs DCS 3 would should a hysteresis loop. With the orientation of the thermocouple leads unknown it was impossible to establish if the hysteresis in the DCS vs RS temperature plots were predominantly because of the heat capacity of the CalDet or whether it was because the thermocouples were not universally oriented. Thankfully the .3%/^{o}C light out was countered with an opposite .2%/^{o}C contribution from the electronics, and so the overall contribution to the CalDet energy resolution was only .1%/^{o}C.

5 Near Detector work

With the beam turn-on and data taking now underway, MINOS is starting to come into bloom as an experiment. Currently, there is enough data for the Near Detector to start making Monte Carlo comparisons as well as properly explore detector response.

Using the March and May 2005 Near Detector data I made a comparison of the reconstructed muon energy between the Monte Carlo and data. The data was taken in one of three three different beam configuration modes: High Energy (HE), Medium Energy (ME) and Low Energy (LE). The data can be broken down into two subcategories relating to the reconstruction method. The first method is used for lower energy muons which stop in the detector and the second is for higher energy muons which leave the detector. The stopping muons are reconstructed as a function of track-length while the exiting muons are reconstructed using track curvature (q/p). The table below as well as the ME March LE histogram fig 8 show the comparison. Little or no data was taken for the ME or HE in March and similarly no LE data has been taken in May, and was therefore not included in the tables below.

Data set	**LE total**	**mean**	**RMS**	**LE q/p**	**mean**	**RMS**	**LE trklngth**	**mean**	**RMS**
March 2005	5290	3.9363	3.8955	2884	5.1226	4.6138	2406	2.5143	2.0348
May 2005	/	/	/	/	/	/	/	/	/
Monte Carlo	15956	3.7420	3.8402	8262	5.0014	4.6457	7694	2.3897	1.9683

Table 1: Medium Energy data and Monte Carlo table for Muon Reconstruction energy.

Data set	**ME total**	**mean**	**RMS**	**ME q/p**	**mean**	**RMS**	**ME trklngth**	**mean**	**RMS**
March 2005	/	/	/	/	/	/	/	/	/
May 2005	25387	3.8012	3.3032	13565	4.6749	3.9465	12272	2.8355	1.9969
Monte Carlo	6970	3.7566	3.0578	3201	4.6033	3.7644	3769	3.0375	2.0322

Table 2: Medium Energy data and Monte Carlo table for Muon Reconstruction energy.

Data set	HE total	mean	RMS	HE q/p	mean	RMS	HE trklngth	mean	RMS
March 2005	/	/	/	/	/	/	/	/	/
May 2005	85173	4.5222	3.8764	46417	5.7566	4.4168	38756	3.0437	2.3766
Monte Carlo	2486	5.1205	3.9705	1261	6.5200	4.5417	1225	3.6798	2.5825

Table 3: High Energy data and Monte Carlo table for Muon Reconstruction energy.

The LE, ME and HE Monte Carlo was a limited subset of all the available Monte Carlo and further analysis will include more reprocessed files. To test that MINOS is acquiring as much data as possible, to go with the millions of events from Monte Carlo, another analysis was undertaken to examine the efficiency of the Near Detector using muon tracks.

Knowing the muon track vertex and end plane it was possible to examine how many planes were hit between the vertex and end plane. Efficiency then becomes $\frac{expected\#hits}{total\#hits}$ for each plane (fig 9). A fiducial volume cut was essential, because in the calorimeter, first 2 meters of the ND, only every 5th plane is fully instrumented while the sandwiched 4 planes are only partially instrumented and do not cover the whole area of the steel. The fiducial volume cut makes sure that tracks detected in the fully instrumented planes 'should' also be detected in the partially instrumented planes. In the Spectrometer section, last 5 meters of the ND, the ONLY instrumented plane occurs every fifth plane and is fully instrumented, and this accounts for most of the planes in the latter half of the ND having a zero efficiency.

6 Summary

Work covering the temperature calibration of CalDet has come to an unfortunate close due an error in assembly of the thermocouples. Thankfully other projects such as doing a comparison between the muon reconstruction energy for Monte Carlo and data have proved more fruitful. The Near Detector was shown to have an efficiency of $\sim$81% and small deviations are going to used for a further study into isolating and solving detector calibration issues. I will also be undertaking a Geant simulation of the Hadron Absorber, which is crudely modelled in the current version of the MINOS software.

7 Plots and Figures

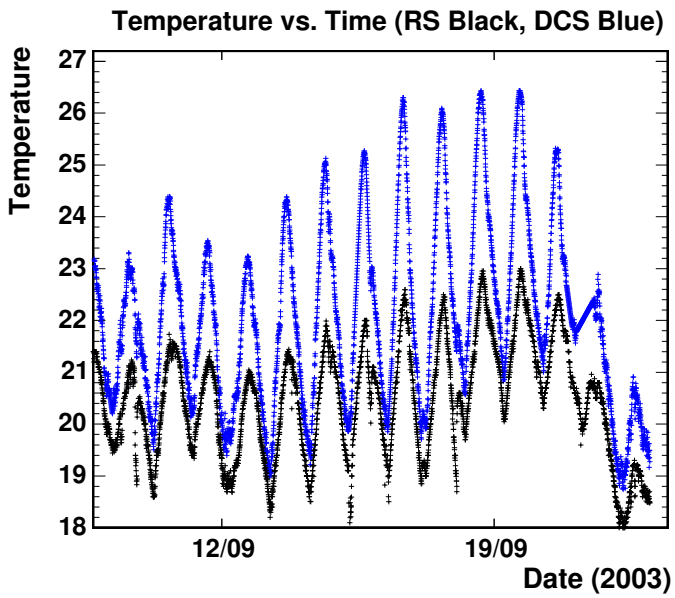

Figure 1: RS and DCS Temperature of a 15 day period of the Near/Far Electronics running at CalDet.

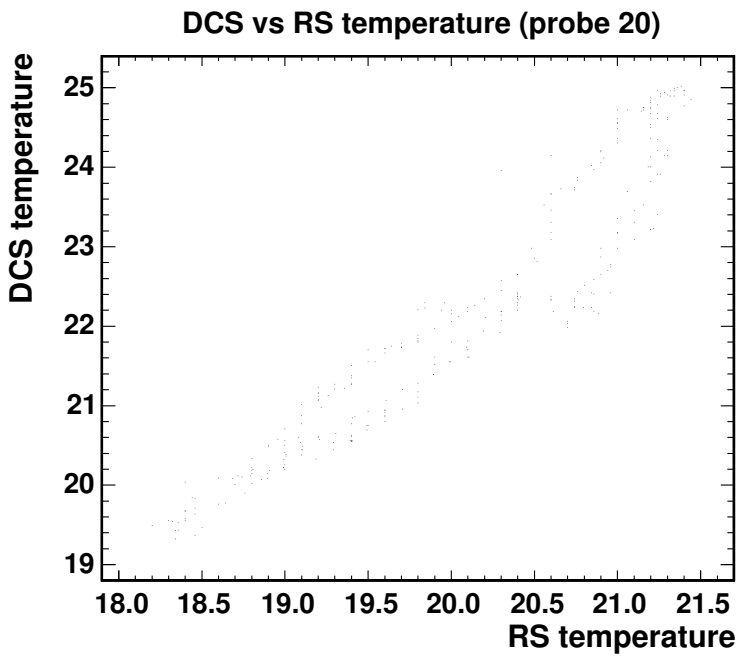

Figure 2: DCS vs RS temperature for Probe 20 over a 24 hours period of the Near/Far Electronics running at CalDet.

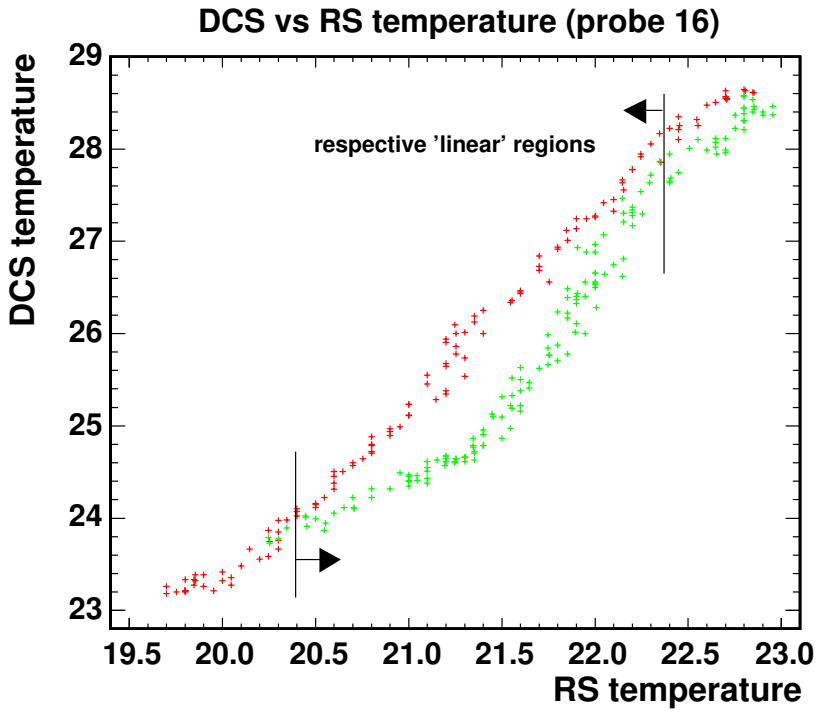

Figure 3: DCS vs RS temperature for Probe 16 over a 24 hours period of the Near/Far Electronics running at CalDet. Red is when the CalDet is heating and Green is when the CalDet is cooling.

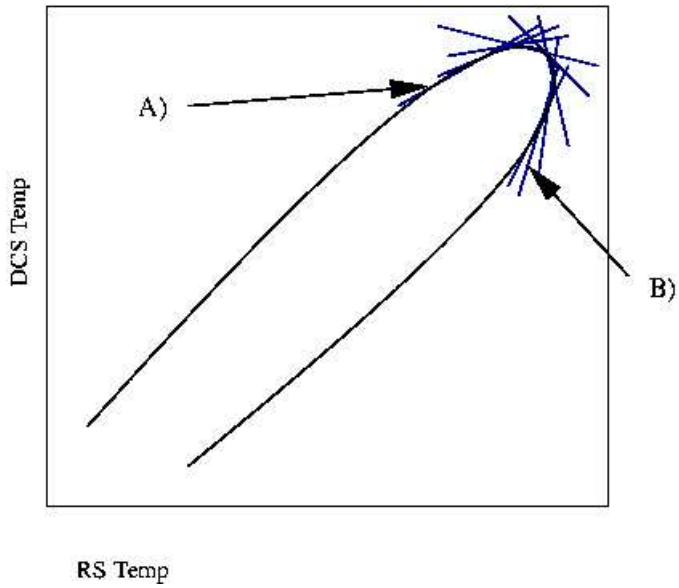

Figure 4: Moving average method for establishing the offset of a hysterisis. Point A is where the X points of the running average leave the heating slope, and point B is where the running average begins to equal the cooling slope.

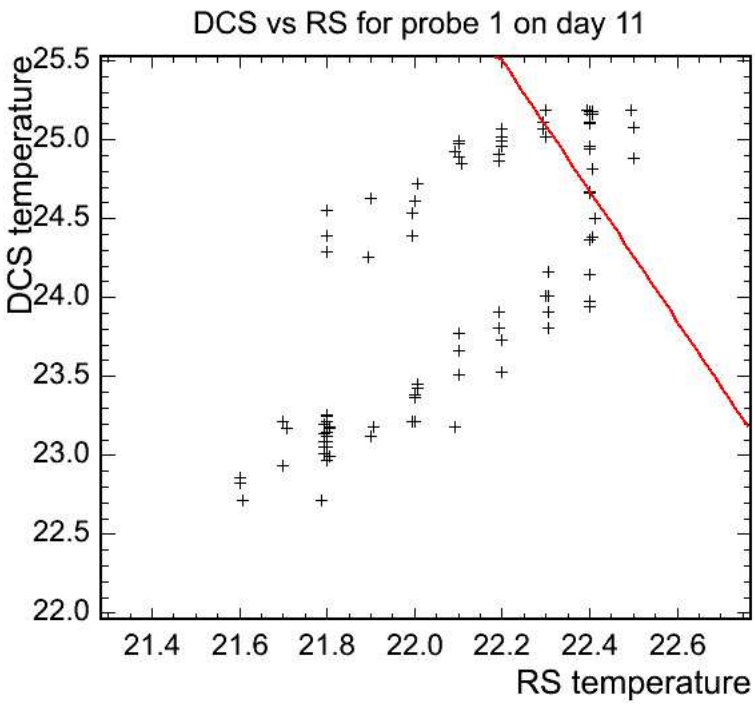

Figure 5: An example of when the moving average works.

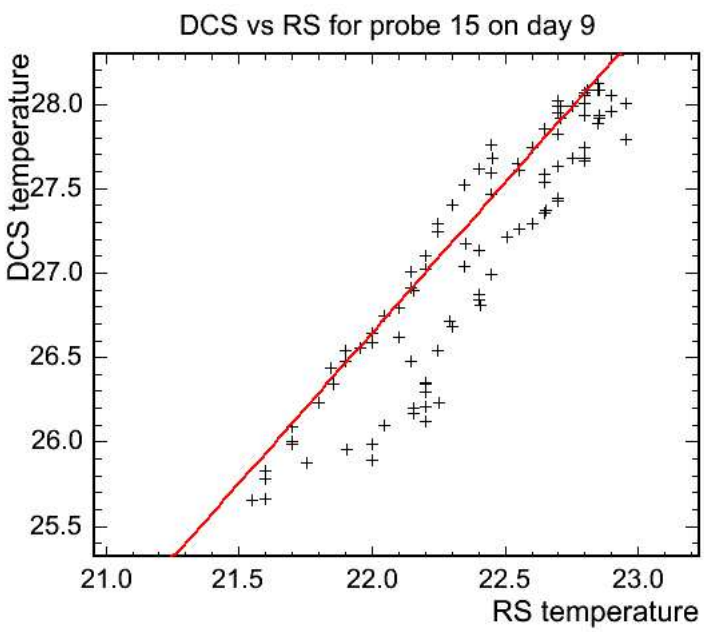

Figure 6: An example of when the moving average does not work.

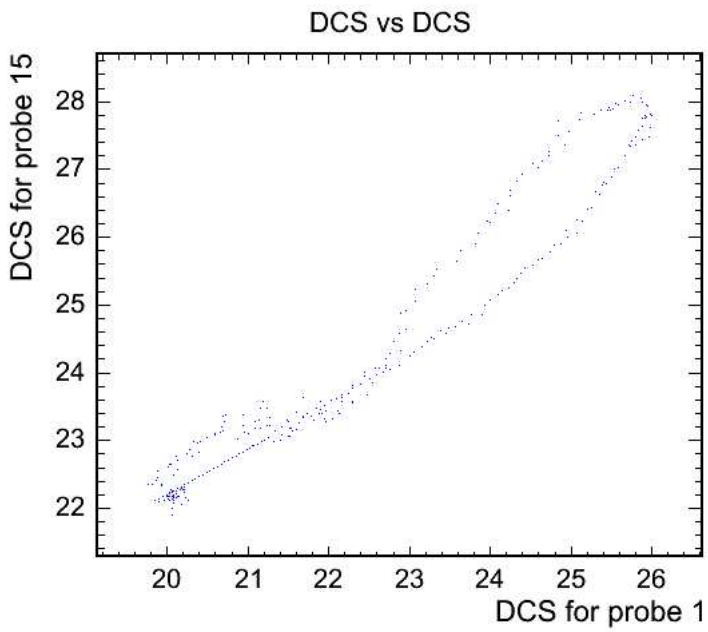

Figure 7: Switched thermocouple leads exhibiting a hysterisis.

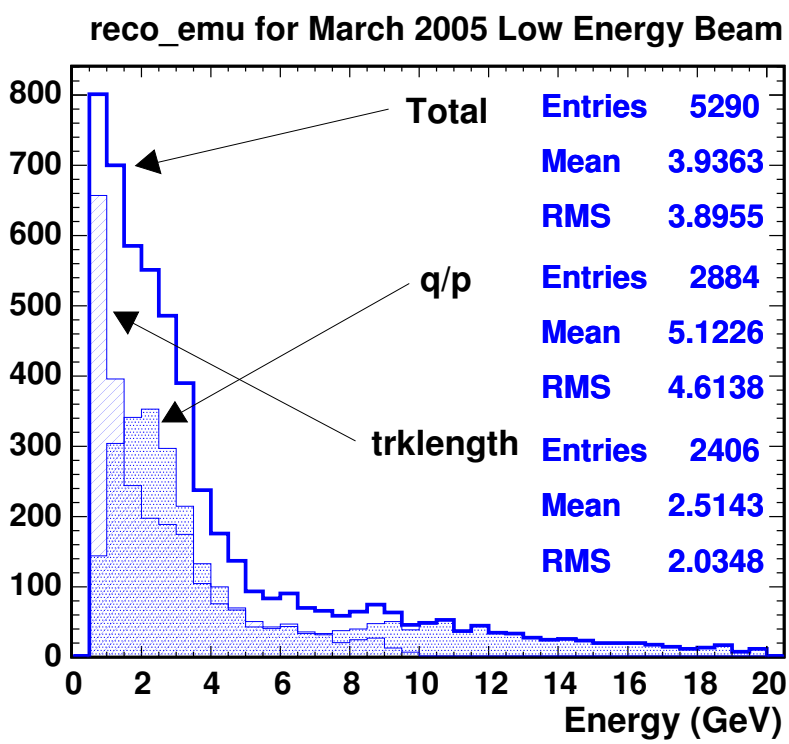

Figure 8: March 2005 reconstructed muon energy separated into energy reconstructed from track length as well as energy reconstructed from curvature.

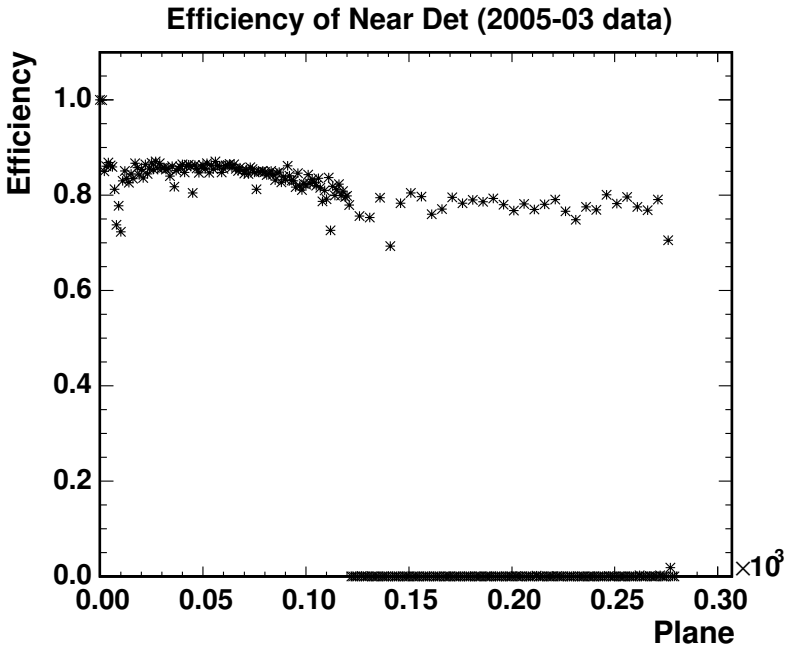

Figure 9: Efficiecny of the Near Detector using muon tracks.

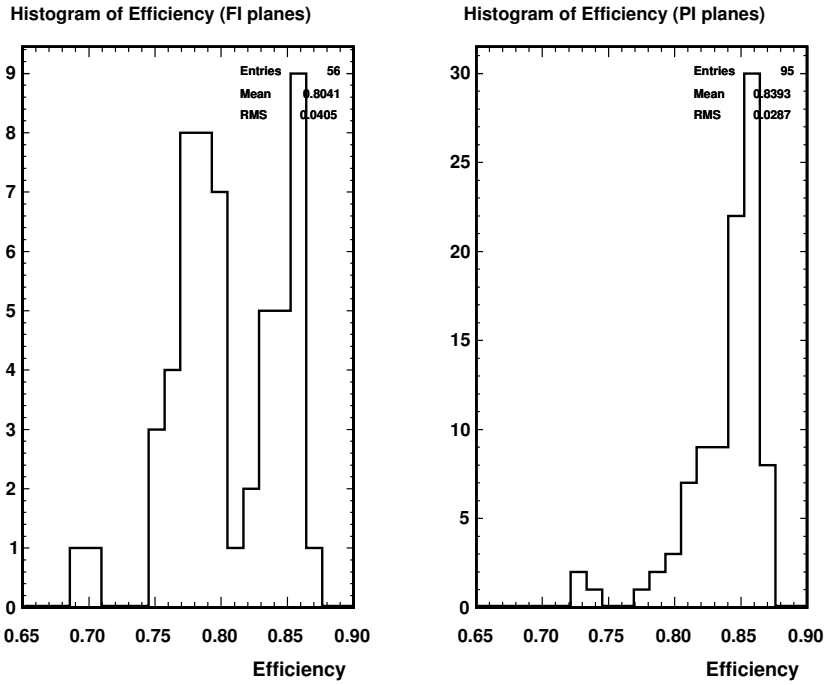

Figure 10: Histograms of the efficiency of the partially and fully instrumented planes of the MINOS Near Detector.

References

[1] Jr. Davis, Raymond, Don S. Harmer, and Kenneth C. Hoffman. Search for neutrinos from the sun. *Phys. Rev. Lett.*, 20:1205–1209, 1968.

[2] Y. Fukuda et al. Evidence for oscillation of atmospheric neutrinos. *Phys. Rev. Lett.*, 81:1562–1567, 1998.

[3] Q. R. Ahmad et al. Measurement of the charged current interactions produced by b-8 solar neutrinos at the sudbury neutrino observatory. *Phys. Rev. Lett.*, 87:071301, 2001.